Developmental Cell
Article

Chemokine Signaling Directs Trunk Lymphatic Network Formation along the Preexisting Blood Vasculature

Young Ryun Cha,[1] Misato Fujita,[1] Matthew Butler,[1] Sumio Isogai,[2] Eva Kochhan,[3] Arndt F. Siekmann,[3] and Brant M. Weinstein[1,*]
[1]Laboratory of Molecular Genetics, National Institute of Child Health and Human Development, National Institutes of Health, 6B/309, 6 Center Drive, Bethesda, MD 20892, USA
[2]Department of Anatomy, School of Medicine, Iwate Medical University, Morioka 020-8505, Japan
[3]Max Planck Institute for Molecular Biomedicine, Roentgenstr. 20, 48149 Muenster, Germany
*Correspondence: bw96w@nih.gov
DOI 10.1016/j.devcel.2012.01.011

SUMMARY

The lymphatic system is crucial for fluid homeostasis, immune responses, and numerous pathological processes. However, the molecular mechanisms responsible for establishing the anatomical form of the lymphatic vascular network remain largely unknown. Here, we show that chemokine signaling provides critical guidance cues directing early trunk lymphatic network assembly and patterning. The chemokine receptors Cxcr4a and Cxcr4b are expressed in lymphatic endothelium, whereas chemokine ligands Cxcl12a and Cxcl12b are expressed in adjacent tissues along which the developing lymphatics align. Loss- and gain-of-function studies in zebrafish demonstrate that chemokine signaling orchestrates the stepwise assembly of the trunk lymphatic network. In addition to providing evidence for a lymphatic vascular guidance mechanism, these results also suggest a molecular basis for the anatomical coalignment of lymphatic and blood vessels.

INTRODUCTION

The lymphatic system is essential for tissue fluid homeostasis and immune surveillance and is important in a number of pathological processes, including inflammation, lymphedema, and tumor metastasis (Alitalo et al., 2005; Oliver and Alitalo, 2005; Tammela and Alitalo, 2010). Like blood vessels (BVs), lymphatic vessels (LVs) assemble into a complex but highly stereotypic and evolutionarily conserved network. The lymphatic network is anatomically separate and distinct from the circulatory system, although larger-caliber LVs and BVs (in particular, arteries) frequently coalign (Gray, 1918; Sabin, 1902, 1909).

The molecular factors regulating emergence of the embryonic lymphatic vasculature have been studied in a number of different vertebrates, in particular in mice, resulting in the identification of key molecules regulating lymphatic specification and differentiation, such as Sox18, Prox1, CoupTFII, VegfC, Vegfr3, and Nrp2 (reviewed in Alitalo et al., 2005; Butler et al., 2009; Oliver and Alitalo, 2005; Tammela and Alitalo, 2010). However, progress has been slowed by the difficulty in imaging lymphatics or in experimentally or genetically manipulating them in most vertebrate model organisms. The zebrafish has been shown to be a valuable model for experimental and genetic analysis and imaging of the blood vascular system (McKinney and Weinstein, 2008), and recent studies have provided evidence that the zebrafish is also useful for studying lymphatic development (Bussmann et al., 2010; Del Giacco et al., 2010; Geudens et al., 2010; Hogan et al., 2009; Küchler et al., 2006; Pedrioli et al., 2010; Saharinen et al., 2010; Yaniv et al., 2006). The zebrafish has a well-defined lymphatic vascular system that shares many of the morphological, molecular, and functional characteristics of the LVs found in other vertebrates (Küchler et al., 2006; Yaniv et al., 2006). A distinct, anatomically conserved system of lymphatics is present with an overall pattern and morphology resembling that found in other developing vertebrates. Furthermore, zebrafish lymphatics express known molecular markers of lymphatic endothelial cell (LEC) fate and require the function of genes known to be important for lymphangiogenesis in mice and other species, including the genes noted previously. Zebrafish lymphatics also drain and collect subcutaneously injected dyes, a key functional feature reported for the lymphatics of other species (Ny et al., 2005; Tilney, 1971). The identification of a lymphatic system in the zebrafish is an important finding, given the accessibility of the fish to forward-genetic analysis and high-resolution in vivo imaging of the vasculature.

As in the blood vascular system, the major vessels of the lymphatic vascular system have a defined, evolutionarily conserved anatomical pattern. Recent work has begun to provide insights into guidance cues directing early patterning of blood vascular networks, many of which are common to those used for the patterning of other tissues and organs, in particular the nervous system (Melani and Weinstein, 2010). However, the mechanisms responsible for guiding the assembly of the lymphatic vascular system and establishing its anatomical form remain largely unknown. A number of zebrafish studies have begun to explore the mechanisms directing lymphatic development and patterning. Imaging and cell lineage tracing studies documented the assembly of the trunk lymphatic system from

posterior cardinal vein (PCV)-derived lymphatic progenitors that form the "parachordal line" (PC), a structure that serves as the source of lymphatic endothelium for all trunk lymphatics (Hogan et al., 2009; Isogai et al., 2003; Küchler et al., 2006; Yaniv et al., 2006). LECs initially emerge from the PC and migrate adjacent to trunk arterial intersegmental blood vessels (aISVs), suggesting that arteries might provide a guidance template (Bussmann et al., 2010; Geudens et al., 2010; Yaniv et al., 2006). The involvement of Notch signaling in this arterial alignment has been proposed (Geudens et al., 2010), but there is evidence for both positive and negative functions for Notch in lymphatic development, and its role remains unclear (see Discussion). Zebrafish studies have highlighted the functional requirement for a number of other factors during trunk lymphatic development. The extracellular matrix-associated protein *collagen* and *calcium-binding EGF domain-1* (*ccbe1*) is required nonautonomously for emergence of lymphatic endothelium from the primitive veins and for lymphatic assembly, probably acting as a permissive factor for lymphatic migration (Hogan et al., 2009). Loss of either *claudin-like protein 24* (*clp24*) or *synectin* leads to defects in lymphatic development in both mice and zebrafish (Geudens et al., 2010; Saharinen et al., 2010). The microRNA *miR-31* has been shown to be required for lymphatic gene expression, differentiation, and sprouting of human LECs and lymphatics in developing *Xenopus* and zebrafish (Pedrioli et al., 2010). The *spleen tyrosine kinase* (*syk*) and related *zeta associated protein-70* (*zap-70*) are required for both angiogenic and lymphatigiogenic development in the fish (Christie et al., 2010).

Although a variety of molecular regulators of lymphatic development have now been identified in mice, zebrafish, and other models, none of these factors has been shown to act as a direct guidance cue guiding lymphatic patterning, in a manner analogous to the way in which neuronal guidance factors, such as semaphorin signaling, direct both neural and vascular patterning (see, e.g., Torres-Vázquez et al., 2004). Here, we provide evidence that migration of chemokine receptor Cxcr4a- and Cxcr4b-positive LEC is guided by chemokine ligands Cxcl12a (SDF1a) and Cxcl12b (SDF1b) expressed in neighboring tissues located along the migration pathways taken by these cells. Our data suggest that chemokine signaling helps direct and orchestrate the stepwise assembly and patterning of the trunk lymphatic network.

RESULTS

Stepwise Assembly of the Trunk Lymphatic Network

The emergence of the lymphatic vascular system of the zebrafish has been described in studies from this and other laboratories (Bussmann et al., 2010; Geudens et al., 2010; Hogan et al., 2009; Küchler et al., 2006; Yaniv et al., 2006). We used confocal and two-photon time-lapse imaging of *Tg(fli1a:EGFP)*^{y1} zebrafish to examine early zebrafish trunk lymphatic development in detail (Figure 1; see also Movie S1 available online). Lymphatic progenitors initially emerge from the PCV as sprouts that grow dorsally near or along vertical intersegmental boundaries (Isogai et al., 2003; Figures 1A–1C). As they reach the horizontal myoseptum (HM), a tissue border dividing the dorsal and ventral halves of the somites, these sprouts turn laterally into the HM, then branch rostrally and caudally, tracking along the superficial HM, near the lateral surface of the trunk to populate the PC (Figures 1D–1K). By 60 hpf, dorsal and ventral sprouts emerge from the PC at aISVs, tracking closely along the aISVs as they grow dorsally and ventrally (Figures 1L–1O). The sprouts grow and extend to form the intersegmental lymphatic vessels (ISLVs). The dorsal sprouts branch rostrally and caudally as they reach the dorsal longitudinal anastomotic blood vessels (DLAVs) to form the dorsal lymphatic lines (DLL), whereas ventral sprouts branch rostrally and caudally just below the dorsal aorta (DA) and just above the PCV to form the lymphatic thoracic duct (TD) (Figures 1P–1R; see also Yaniv et al., 2006). It is important to reiterate that the ISLVs that branch and grow dorsally and ventrally from the PC do so only along aISVs, not along venous intersegmental blood vessels (vISVs) (Figures 1S and 1T; also noted previously in Yaniv et al., 2006 and more recently in Bussmann et al., 2010; Geudens et al., 2010). The complete series of steps of trunk lymphatic network assembly described previously are visualized in the two-photon time-lapse imaging sequence shown in Movie S1. This and previously published (Yaniv et al., 2006) time-lapse imaging movies show that developing trunk lymphatics grow and extend as continuous vascular sprouts, in a similar manner to angiogenic BVs. Expression of Prox1, a specific marker of lymphatic endothelium (Wigle and Oliver, 1999), is detected in lymphatic progenitors and LEC at each stage of trunk lymphatic network development beginning from their appearance as individual cells within the PCV (Figure 1K; Figure S1).

Chemokine Receptor *Cxcr4a* Is Expressed in LEC

Chemokine signaling plays a role in cellular guidance and patterning in various tissues (Bussmann et al., 2011; David et al., 2002; Doitsidou et al., 2002; Fujita et al., 2011; Ghysen and Dambly-Chaudière, 2007; Haas and Gilmour, 2006; Knaut et al., 2003; Nair and Schilling, 2008; Siekmann et al., 2009). Examination of the expression pattern of zebrafish chemokine receptors suggested that some of them might be involved in directing the assembly of the trunk lymphatic network (Figure 2). The chemokine receptor *cxcr4a* is expressed in developing lymphatic endothelium. Whole-mount in situ hybridization (WISH) shows that *cxcr4a* is initially expressed in the DA and in the primary intersegmental blood vessel (ISV) sprouts emerging from it (Figures 2A and 2B). However, *cxcr4a* expression is rapidly extinguished in trunk BVs after this stage, and *cxcr4a* becomes expressed in developing lymphatics, including the PC (Figures 2F and 2G) and ISLVs (Figures 2J and 2K). Higher-magnification WISH images indicate that *cxcr4a* is indeed expressed in LECs (Figure 2N). This is confirmed by high-resolution confocal imaging of vessels in *Tg(fli1a:EGFP)*^{y1} animals injected with a recombineered bacterial artificial chromosome (BAC) transgene containing the *cxcr4a* promoter upstream of TagRFP-T (Figures 2C–2E, 2H, 2I, 2L, 2M, and 2O; Figures S2A–S2I). TagRFP-T expression (red/yellow) is detected in endothelial cells (ECs) of the DA and primary ISVs, where endogenous *cxcr4a* is initially expressed (Figures S2B–S2E and S2I), as well as in some ECs in the PCV, where lymphatic progenitors emerge (Figure S2I). TagRFP-T expression is also detected in lymphatic progenitors sprouting from the PCV (arrowheads in Figures 2C–2E; arrowheads in

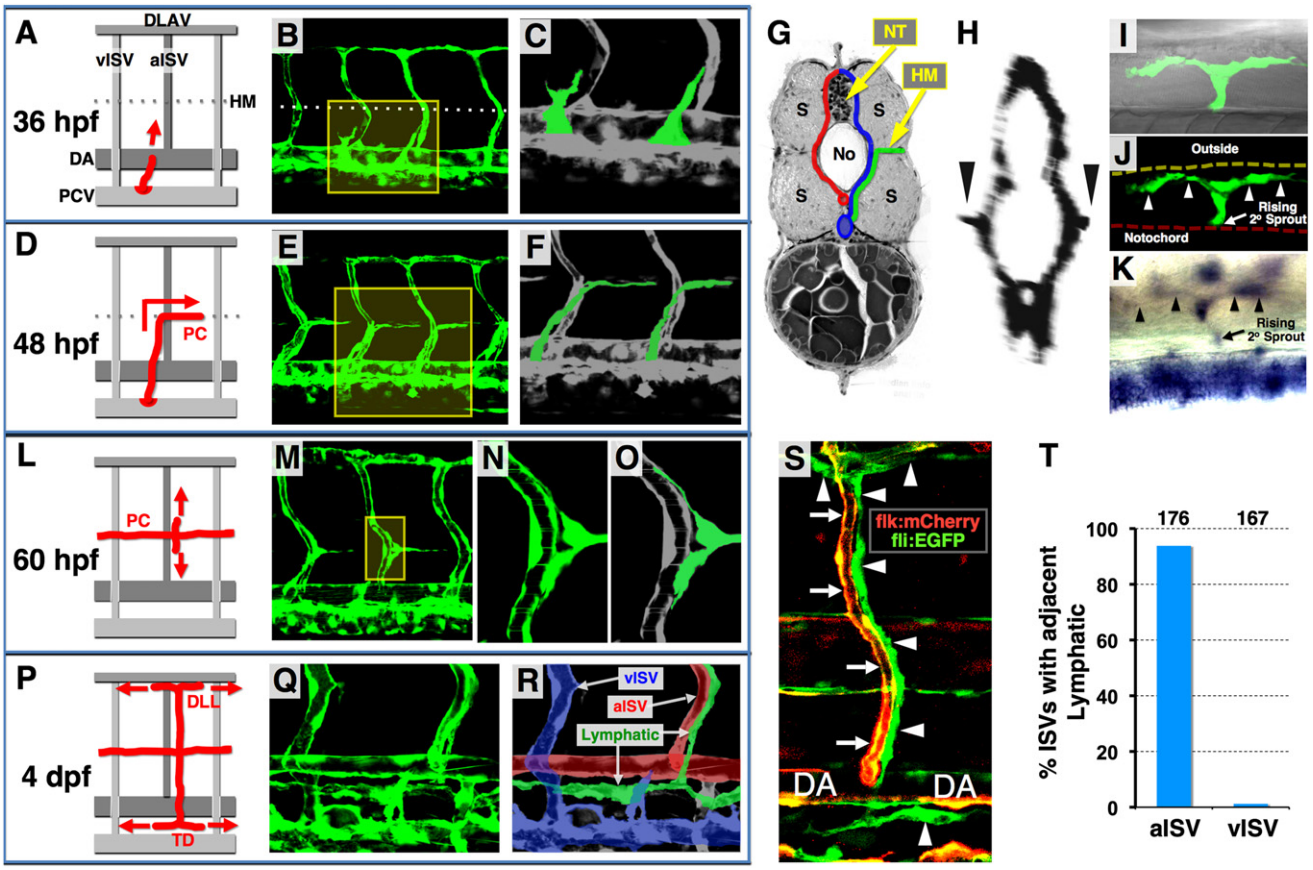

Figure 1. Anatomy and Assembly of the Trunk Lymphatic Network in the Developing Zebrafish

(A, D, L, and P) Diagrams illustrating successive steps in trunk lymphatic network assembly at different developmental stages (red, developing lymphatics; red arrows, their growth direction).

(B, E, M, and Q) Confocal images of the vasculature in *Tg(fli1a:EGFP)*^{y1} animals at each stage (yellow boxes, magnified areas shown to the right).

(C, F, N, and O) Magnified views of the boxed portions of the images to the left (green, developing lymphatic vessels, except N).

(G) Cross-sectional diagram illustrating lateral growth of lymphatic progenitors (green) toward the superficial HM (red, arterial BVs; blue, venous BVs; No, notochord; NT, neural tube; S, somites).

(H) Cross-sectional reconstruction (rotated 90°) of confocal stacks used in (E) (arrowheads, vascular spouts extending laterally along the HM).

(I and J) Dorsal view confocal/DIC (I) and confocal only (J) images of a single branching PC sprout (arrowheads) in the superficial HM of a 60 hpf *Tg(fli1a:EGFP)*^{y1} larva.

(K) Dorsal view image of a branching PC sprout (arrowheads) in the superficial HM of a 56 hpf larva WISH-stained for *prox1*.

(R) Color-coded image of (Q) (green, lymphatic vessels; red, arterial BVs; blue, venous BVs).

(S) Confocal image of an aISVs (red/yellow, arrows) with a coaligned ISLV and other developing lymphatics (green, arrowheads) in a 3 dpf *Tg(flk:mCherry), Tg(fli1a:EGFP)*^{y1} double transgenic animal.

(T) Quantification of aISV and vISV (determined by observing vessels using confocal microscopy at 5 dpf) with a coaligned ISLVs. The total number of aISVs or vISVs counted is shown above each bar.

See also Movie S1 and Figure S1.

Figures S2B and S2C), in lymphatic sprouts generating the PC (arrowheads in Figures 2H and 2I), in the PC (arrows in Figures 2H and 2I; arrows in Figures S2F–S2H), in LEC migrating dorsally and ventrally from the PC (arrowheads in Figures 2L and 2M), and in the TD (arrowheads in Figure 2O) with relatively high frequency (Figure S2I). In addition to *cxcr4a,* we found that the related chemokine receptor *cxcr4b* is also expressed in the developing lymphatic endothelium (Figures S2J–S2N). Higher-magnification WISH images revealed *cxcr4b* expression in selected cells in the PCV (black arrows in Figures S2J and S2K), in lymphatic sprouts from the PCV (white arrow in Figure S2K), in LEC migrating dorsally and ventrally from the PC (arrows in Figure S2L), and in the developing TD (arrows in Figures S2M and S2N).

Cxcl12 Ligands Are Expressed in Tissues Adjacent to Migrating LEC

Previous work has documented that Cxcl12a and Cxcl12b are ligands for Cxcr4a and Cxcr4b in the zebrafish (Bussmann et al., 2011; Chong et al., 2007; Fujita et al., 2011; Nair and Schilling, 2008; Siekmann et al., 2009). We observe expression of these ligands adjacent to the paths taken by growing Cxcr4a/b-positive trunk lymphatics. WISH shows that *cxcl12a* is initially expressed in the superficial HM toward which

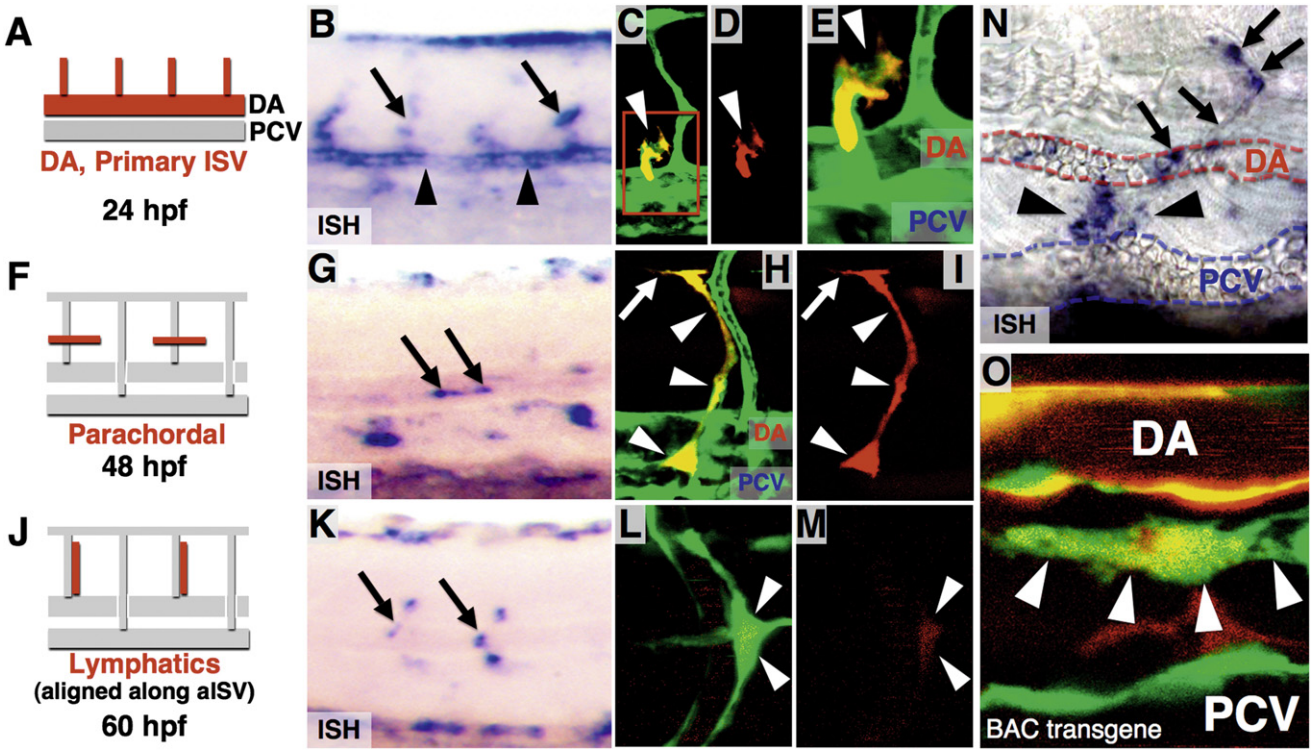

Figure 2. Chemokine Receptor *Cxcr4a* Expression in the Developing Zebrafish Trunk

(A, F, and J) Diagrams indicating *Cxcr4a* expression domains as red at stages shown below.

(B, G, and K) WISH images corresponding to left panels (arrows, *Cxcr4a* expression domains; arrowheads, *Cxcr4a* expression in DA at 24 hpf).

(C–E) Confocal images of a 35 hpf *Tg(fli1a:EGFP)*^{y1} embryo (green) injected with a recombineered BAC clone with TagRFP-T driven by the *cxcr4a* promoter (red). TagRFP-T is detected in lymphatic progenitors sprouting from the PCV. (C) Merged image. (D) Red channel only. (E) Magnified view in the red box of (C).

(H and I) Confocal images of a 45 hpf *Tg(fli1a:EGFP)*^{y1} embryo (green) injected with a recombineered BAC clone with TagRFP-T driven by the *cxcr4a* promoter (red). TagRFP-T is detected in sprouting lymphatic progenitors forming the PC. (H) Merged image. (I) Red channel only.

(L and M) Confocal image of a 62 hpf *Tg(fli1a:EGFP)*^{y1} embryo (green) injected with a recombineered BAC clone with TagRFP-T driven by the *cxcr4a* promoter (red). TagRFP-T is detected in LEC migrating dorsally and ventrally from the PC. (L) Merged image. (M) Red channel only.

(N) High-magnified WISH image showing a *cxcr4a*-expressing TD sprout extending along the intersegmental boundary (arrows) and between the DA and PCV (arrowheads) at a 3 dpf animal.

(O) Confocal image of ventral trunk vessels in a 5 dpf *Tg(fli1a:EGFP)*^{y1} embryo (green) injected with a recombineered BAC clone with TagRFP-T driven by the *cxcr4a* promoter (red). TagRFP-T expression is present in both TD (arrowheads) and DA, but not in the PCV.

See also Figure S2.

PCV-derived lymphatic progenitors migrate and along which they form the PC (Figures 3A–3D). HM expression of *cxcl12a* is extinguished at later stages, when ISLV sprouts begin to exit the PC, and *cxcl12a* becomes expressed instead in the PCV, particularly the dorsal aspect of the PCV immediately below where the ventral ISLV sprouts grow and branch to form the TD (Figures 3E–3H). At 3 dpf, trunk expression of *cxcl12b* is restricted almost exclusively to aISVs, along which the ISLVs are migrating, although weak expression is also seen in the DA immediately above where the ventral ISLVs will branch to form the TD (Figures 3I and 3J). We verified that *cxcl12b* expression is in aISVs but not in vISVs by examining *cxcl12b* expression in individual WISH-stained animals in which we had previously determined the arterial or venous identity (based on blood flow) of each of the ISVs on both sides of the trunk (Figure 3K; Figure S3A; Movie S2). We also confirmed that *cxcl12b* is expressed in the ECs of the aISVs and DA, but not in adjacent ISLVs, using high-resolution confocal imaging of vessels in *Tg(fli1a:EGFP)*^{y1} animals injected with a recombineered BAC transgene containing the *cxcl12b* promoter upstream of TagRFP-T (Figures 3L and 3M; Figures S3B–S3G). Together, our expression data suggest that Cxcr4a/b-positive lymphatic progenitors/cells might assemble a lymphatic network by migrating toward and/or along Cxcl12a- or Cxcl12b-expressing tissues.

Chemokine Signaling Is Required for Distinct Steps of Lymphatic Network Formation

We performed loss-of-function studies using morpholino oligonucleotides (MO) previously shown to efficiently knock down Cxcr4a, Cxcl12a, and Cxcl12b in the zebrafish (Chong et al., 2007; Hollway et al., 2007; Knaut et al., 2003) to determine whether the function of these genes is required for formation of the trunk lymphatic network (Figures 4A–4K). MO knockdown of either Cxcr4a (Figures 4D and 4E) or Cxcl12a (splice-blocking Cxcl12a MO1; Figures 4F and 4G) leads to loss of the PC (white arrows in Figure 4B) at 55 hpf, and loss of the TD (yellow arrow in

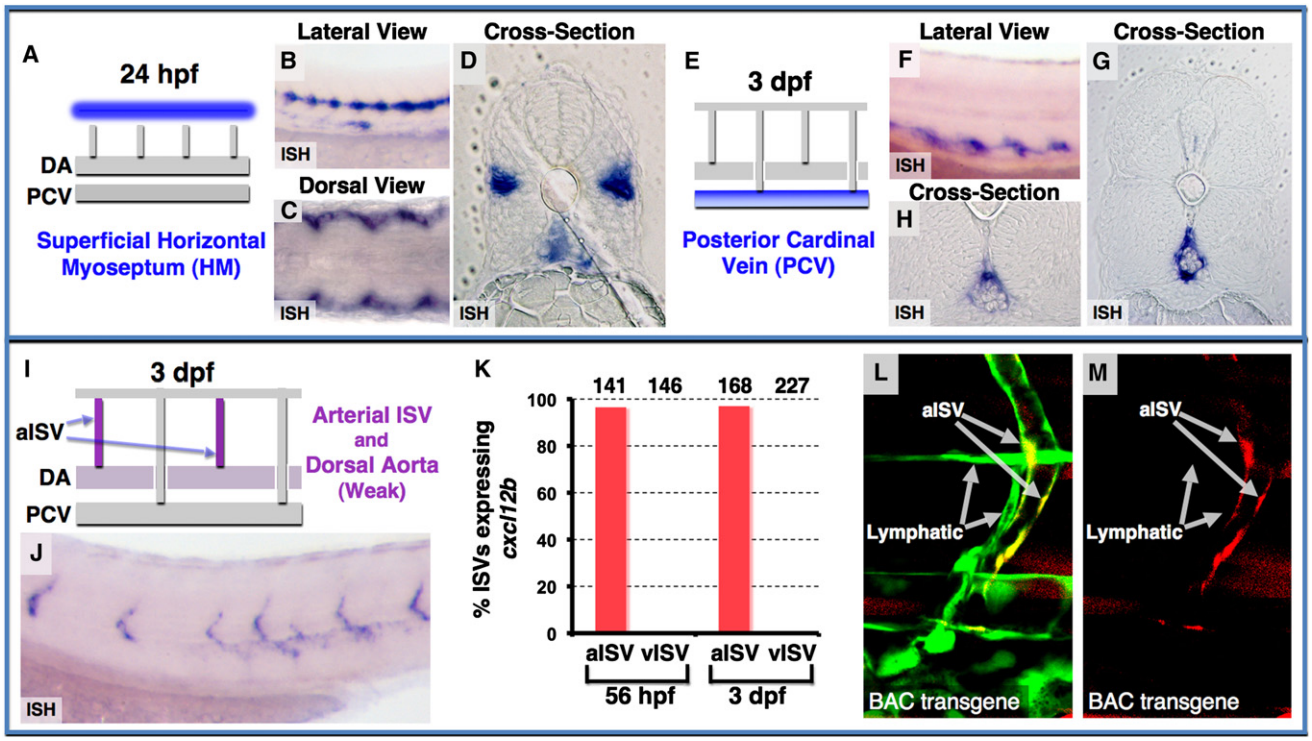

Figure 3. Chemokine Ligand *Cxcl12* Expression in the Developing Zebrafish Trunk

(A–D) *Cxcl12a* expression in the superficial HM at 24 hpf, as shown in diagram (blue in A), and in WISH lateral view (B), dorsal view (C), and cross-section (D).

(E–H) *Cxcl12a* expression in the PCV at 3 dpf, as shown in diagram (blue in E), and in WISH lateral view (F) and cross-sections (G and H).

(I and J) *Cxcl12b* expression in the aISV and DA, as shown in diagram (magenta in I) and in WISH lateral view image (J) at 3 dpf.

(K) Quantification of aISV and vISV (determined by direction of blood flow and by connection to either the DA or PCV as shown in Movie S2) expressing *cxcl12b* at 56 hpf and 3 dpf. Numbers of counted aISVs or vISVs at each time point are indicated above the bars.

(L and M) Confocal images of mid-to-ventral trunk vessels in a 3 dpf *Tg(fli1a:EGFP)*^{y1} embryo (green) injected with a recombineered BAC clone with TagRFP-T driven by the *cxcl12b* promoter (red), showing green and red fluorescence together (L), or red fluorescence only (M). TagRFP-T expression is present in aISVs, but not in adjacent LVs.

See also Figure S3.

Figure 4C) at 5 dpf. Embryos injected with a *Cxcl12a* translation-blocking MO (Cxcl12a MO2) (Doitsidou et al., 2002) also displayed lymphatic defects (Figures S4A–S4F) that were indistinguishable from those in embryos injected with Cxcl12a MO1 (Figures 4F and 4G). MO knockdown of Cxcl12b does not cause any defects in PC formation (Figure 4H) but does cause loss of the TD at later stages (Figure 4I). All of these results were confirmed by quantitative analysis (Figures 4J and 4K). Although a PC is not formed in Cxcl12a and Cxcr4a morphants, vascular sprouts still emerge from the PCV and grow dorsally to the level of the HM (purple arrowheads in Figures 4D and 4F; Figure S4B). We visualized this sprouting more clearly using a Plcg1 morphant background (Lawson et al., 2003) in which primary DA-derived ISV sprouts do not form but secondary PCV-derived sprouts and PC form normally (Figures S4G–S4I). In Cxcl12a/Plcg1, double morphants PCV-derived sprouts form and grow dorsally to the level of the HM, but they fail to form PC along the superficial HM (Figures S4H and S4I). These results suggest that chemokine signaling is not involved in the PCV-derived sprouting and migration to the level of the HM. We further verified an endothelial-specific functional requirement for Cxcr4a for trunk lymphatic development by performing a transgenic rescue experiment (Figures 4L and 4M). Ecdysone-inducible, endothelial-specific overexpression of Cxcr4a using the *fli1a* promoter in animals injected with a bidirectional expression construct (Figure 4L; see Supplemental Experimental Procedures for further description) rescues the majority of PC formation defects in Cxcr4a morphants, despite mosaic expression of injected transgenes (Figure 4M). In addition to defects in ventral ISLV growth and TD formation, Cxcl12b- or Cxcr4a-deficient animals also show defects in dorsal ISLV formation (Figures S4J–S4O).

We further analyzed the functions of chemokine signaling for lymphatic network formation in Cxcr4a mutant, Cxcl12b mutant (Bussmann et al., 2011), and Cxcl12a *medusa* mutant (Valentin et al., 2007) animals (Figures 5A–5E). The *cxcl12a*^{t30516} mutant has a G to A base change creating a premature stop at codon 33 removing the last two-thirds of the protein (Valentin et al., 2007), the *cxcl12b*^{mu100} mutant has a frameshift in the cxcl12b coding sequence after 37 amino acids with a stop codon 23 amino acids later (Bussmann et al., 2011), and the *cxcr4a*^{um21} mutant has a frameshift in the *cxcr4a* coding sequence after 79 amimo acids with a stop codon 32 amino acids later (Bussmann et al., 2011). As in Cxcl12a, Cxcl12b, or Cxcr4a morphants (Figures 4E, 4G, 4I, and 4K; Figures S4D and S4F), TD formation

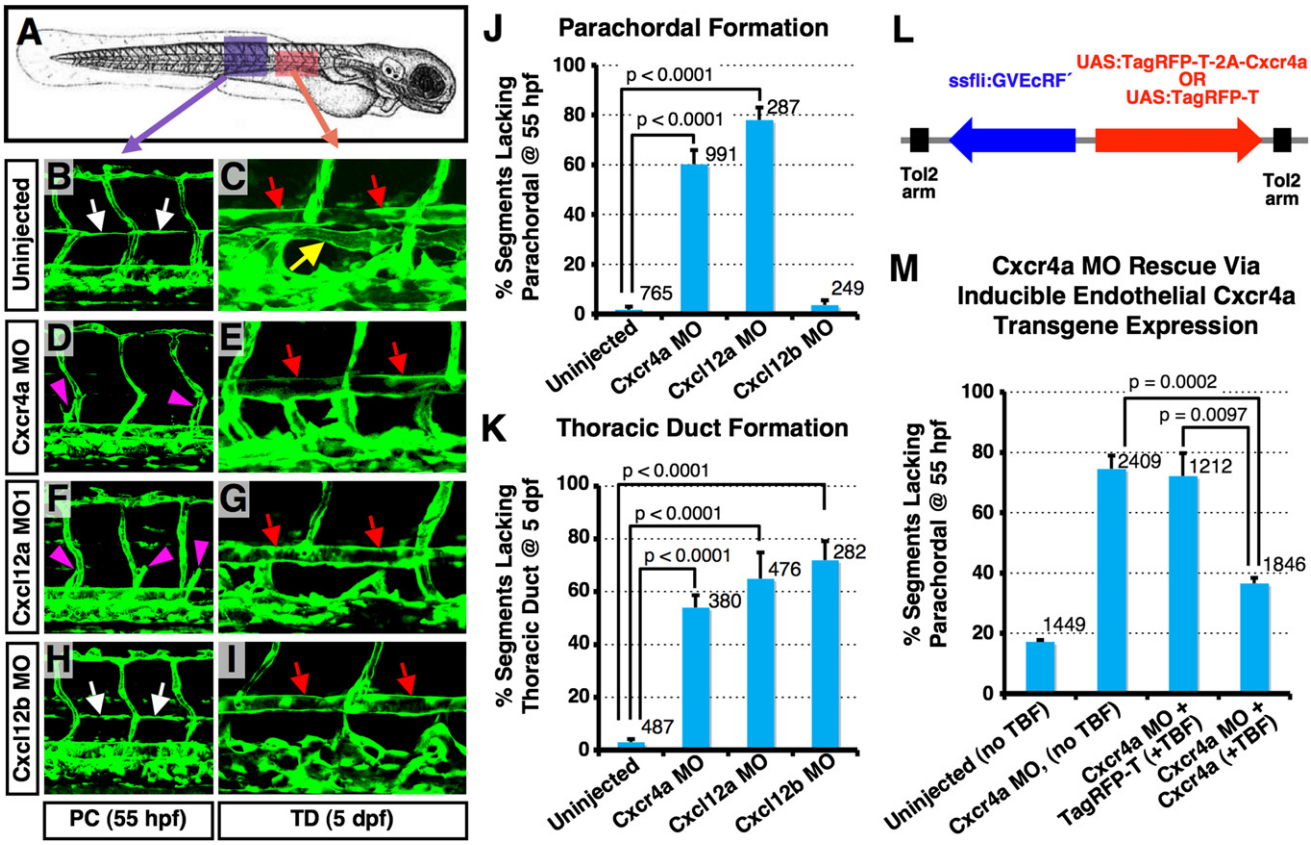

Figure 4. Lymphatic Network Formation Is Disrupted in Chemokine Morphants

(A) Diagram of a zebrafish embryo (a purple box, the region shown in B, D, F, and H; a red box, the region shown in C, E, G, and I).

(B–I) Confocal images of trunk vessels in 55 hpf (B), (D), (F), and (H) or 5 dpf (C), (E), (G), and (I) *Tg(fli-EGFP)*^{y1} embryos that were either not injected, or injected with MOs indicated at left.

(J) Quantification of the PC formation defect in 55 hpf MO-injected embryos (as shown in B, D, F, and H). Values are the mean ± SEM. Numbers of counted PC segments are indicated above the bars.

(K) Quantification of the TD formation defect in 5 dpf MO-injected embryos (as shown in C, E, G, and I). Values are the mean ± SEM. Numbers of counted TD segments are indicated above the bars.

(L) Diagram of Cxcr4a rescue constructs for spatiotemporal overexpression of either TagRFP-T + Cxcr4a or TagRFP-T alone (arrows, direction of gene expression).

(M) Quantification of the PC formation defect in control (column 1) or Cxcr4a morphant animals (columns 2–4), some of which were coinjected with transgenes for ecdysone-inducible endothelial-specific overexpression of either TagRFP-T (column 3) or Cxcr4a (column 4). Values are the mean ± SEM. Numbers of counted PC segments are indicated above the bars. White arrows, PC; yellow arrow, TD; red arrows, DA; magenta arrowheads, secondary sprouts migrating to the level of the HM.

See also Figure S4.

is compromised in either *cxcl12a*^{t30516} or *cxcl12b*^{mu100} ligand mutants, or the *cxcr4a*^{um21} receptor mutant (Figures 5B–5E).

To further clarify the temporal requirement for Cxcr4 function during lymphatic network formation, we treated zebrafish embryos with a known specific Cxcr4 inhibitor, TF10416 (4F-benzoyl-TN14003), previously used in mice (Tamamura et al., 2003a, 2003b). Inhibitor treatment from 30 to 55 hpf results in loss of the PC at 55 hpf (Figures 5F, 5H, and 5J), as well as loss of the TD at later stages (data not shown), although emergence of lymphatic sprouts from the PCV and migration of sprouts to the level of the HM are normal (Figure 5H), as shown previously for Cxcr4a and Cxcl12a morphants (magenta arrowheads in Figures 4D and 4F; Figure S4B). Inhibitor treatment from 3 to 5 dpf, beginning after PC formation is complete, still results in loss of the TD at 5 dpf (Figures 5G, 5I, and 5K). These results suggest that Cxcr4a function is required independently for both early (PC) and later (TD) stages of trunk lymphatic network formation and that loss of TD formation following Cxcr4a knockdown is not merely a secondary consequence of earlier loss of the PC. This notion is supported by the finding that PC-positive Cxcr4a MO-injected animals (Figure S5A) often lack a TD at later stages (Figure S5B). Taken together, our loss-of-function data show that chemokine signaling is required for at least two distinct steps of trunk lymphatic network formation.

Because a recent study reported that netrin1a-mediated guidance of motoneuron axons into the HM is also required for PC formation (Lim et al., 2011), we examined whether these

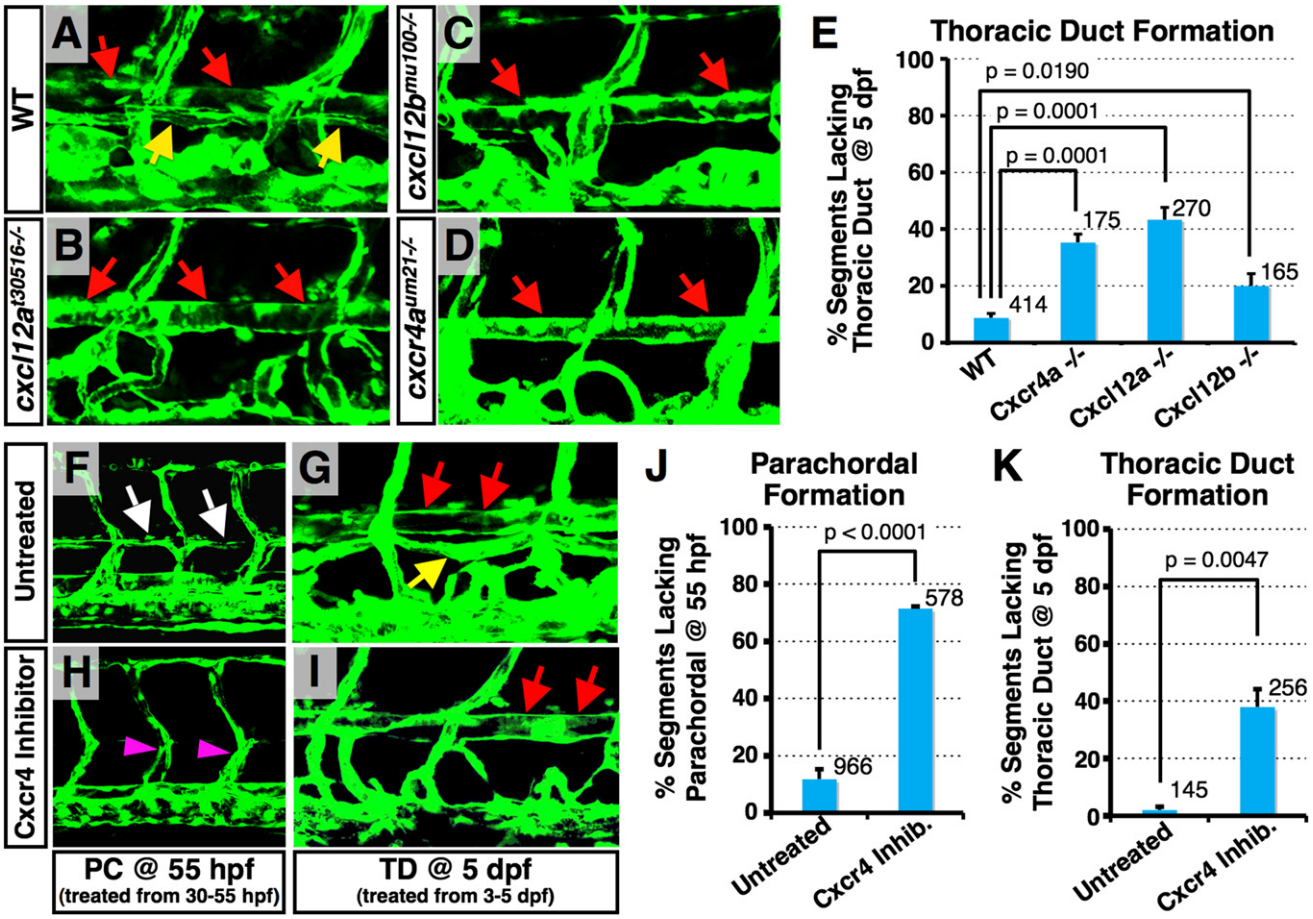

Figure 5. Deficiency of Chemokine Signaling Results in the Loss of Lymphatic Network

(A–D) Confocal images of trunk vessels in 5 dpf *Tg(fli-EGFP)*^{y1} wild-type (A), *cxcl12a*$^{t30516-/-}$ (B), *cxcl12b*$^{mu100-/-}$ (C), and *cxcr4a*$^{um21-/-}$ (D) homozygous mutant animals. Red and yellow arrows indicate DA and TD, respectively.

(E) Quantification of TD formation defect in 5 dpf mutant animals. Values are the mean ± SEM. Numbers of counted TD segments are indicated above the bars.

(F–I) Confocal images of trunk vessels in 55 hpf *Tg(fli-EGFP)*^{y1} animals treated from 30 to 55 hpf (F) and (H) or 5 dpf *Tg(fli-EGFP)*^{y1} animals treated from 3 to 5 dpf (G) and (I) with either DMSO vehicle (F) and (G) or Cxcr4 inhibitor (H) and (I).

(J) Quantification of the PC formation defect in 55 hpf DMSO vehicle or Cxcr4 inhibitor-treated embryos. Values are the mean ± SEM.

(K) Quantification of the TD formation defect in 5 dpf DMSO vehicle or Cxcr4 inhibitor-treated embryos. Values are the mean ± SEM. In (J) and (K), numbers of counted PC or TD segments are indicated above the bars.

See also Figure S5.

two signaling pathways might cooperate during trunk lymphatic network formation by performing combined knockdown using submaximal MO doses. Indeed, double knockdown of Netrin1a and Cxcr4a more strongly suppresses early PC formation (Figure S5C) and later TD formation (Figure S5D) than either Netrin1a or Cxcr4a knockdown alone. In addition, since Cxcr4b is also expressed in the developing lymphatic endothelium (Figures S2J–S2N), we examined whether the Cxcr4a and Cxcr4b receptors also cooperate during trunk lymphatic network formation by using combined knockdown with submaximal MO doses. Again, we found that double knockdown of Cxcr4a and Cxcr4b more strongly suppresses early PC formation (Figure S5E) and later TD formation (Figure S5F) than either Cxcr4a or Cxcr4b knockdown alone. These two sets of data suggest that a number of partially redundant mechanisms are acting in concert to direct trunk lymphatic patterning.

Chemokines Direct the Migration and Alignment of LEC

We performed additional gain-of-function studies to examine whether Cxcl12a and Cxcl12b ligands attract and/or align the growth of developing lymphatics in vivo. We generated bidirectional expression constructs in which a chimeric tebufenozide (TBF)-inducible Gal4-VP16-EcRF′ (GV-EcRF′) transactivator (Esengil et al., 2007) is placed under the control of either *shh*- (for neural floor plate expression) or *fli1a* (for endothelial expression)-derived promoter-enhancers and used to drive UAS-dependent transgene expression. Constructs were injected into *Tg(fli1a:EGFP)*^{y1} animals for TBF-inducible ectopic neural floor plate (FP) expression of either Cxcl12a + TagRFP-T, or TagRFP-T alone (Figures 6A–6H), or for TBF-inducible ectopic panendothelial expression of either Cxcl12b + TagRFP-T, or TagRFP-T alone (Figures 6I–6M; Figure S6).

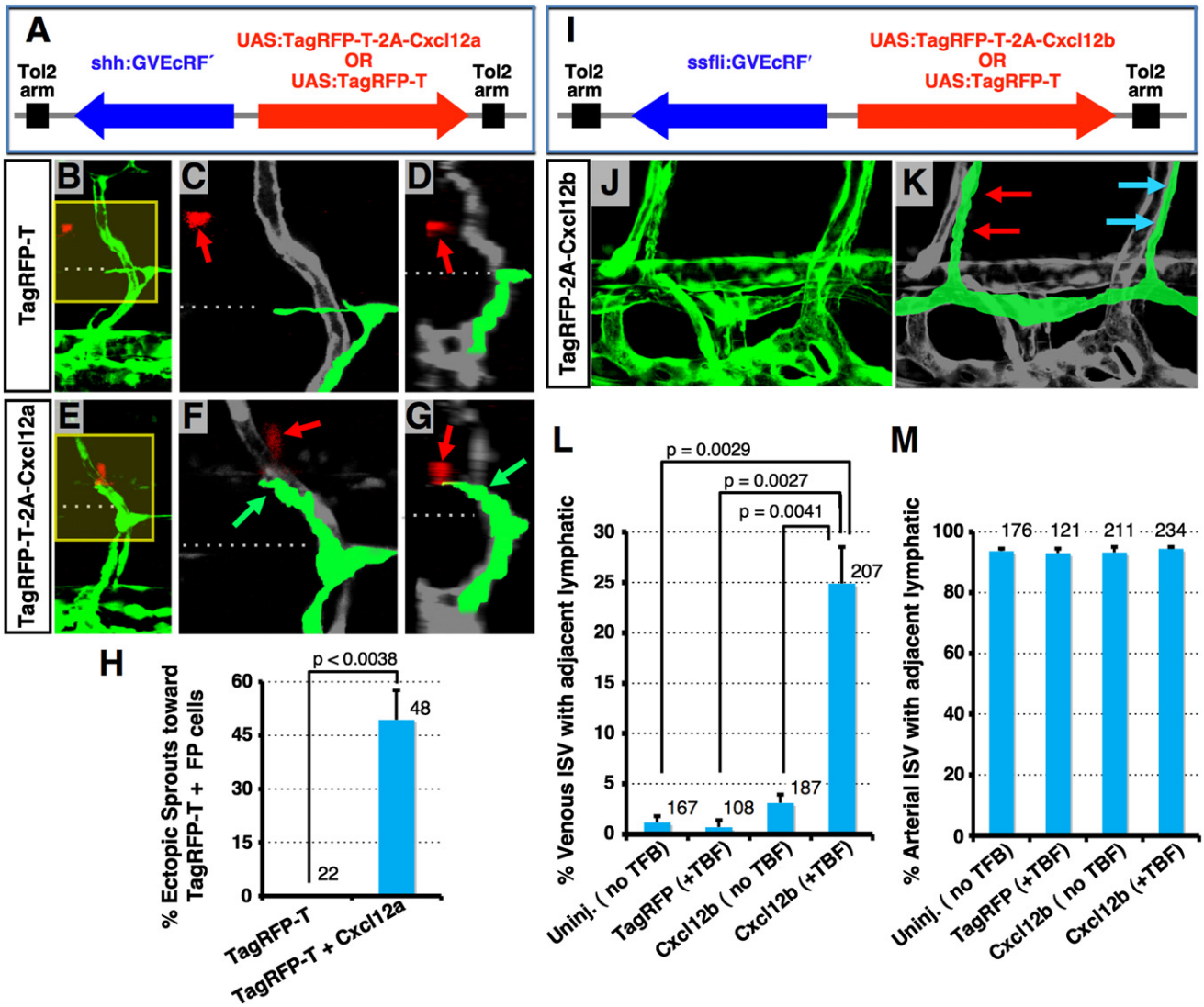

Figure 6. Ectopic Overexpression of Chemokine Ligands Induces Abnormal Migration of LEC

(A) Diagram of constructs for spatiotemporal overexpression of either TagRFP-T + Cxcl12a (produced cotranslationally using a viral 2A peptide linker) or TagRFP-T alone (arrows indicate direction of gene expression; see Supplemental Experimental Procedures for details).

(B–G) Confocal images of trunk vessels in 55 hpf *Tg(fli-EGFP)*^{y1} embryos injected with constructs as shown in (A) and treated with TBF from 30 hpf (see Supplemental Experimental Procedures). Yellow boxes in (B) and (E) indicate areas magnified in (C) and (F), respectively. Images in (D) and (G) are 3D reconstructed cross-sectional views of the same confocal data shown in (B) and (E), respectively (90° horizontal rotation). Dashed lines mark the level of the HM, where the PC normally forms. Red fluorescence (noted with red arrows) shows neural FP cells expressing TagRFP-T (B)–(D) or TagRFP-T + Cxcl12a (E)–(G). Developing lymphatics are colorized green in (C), (D), (F), and (G). Green arrows in (F) and (G) point to an ectopic lymphatic sprout extending dorsally beyond the HM toward nearby TagRFP-T + Cxcl12a-expressing FP cells.

(H) Quantification of ectopic lymphatic sprout migration in segments with TagRFP-T-positive cells in embryos injected with the constructs shown in (A). Values are the mean ± SEM. The total number of secondary sprouts counted is shown above each bar.

(I) Diagram of constructs for spatiotemporal overexpression of either TagRFP-T + Cxcl12b or TagRFP-T alone (arrows, direction of gene expression; see Supplemental Experimental Procedures).

(J) Confocal image of ventral trunk vessels in a 5 dpf *Tg(fli-EGFP)*^{y1} embryo injected with TagRFP-T + Cxcl12b expression construct (shown in I) and treated with TBF from 55 hpf (see Supplemental Experimental Procedures).

(K) Same image as in (J) with developing lymphatics colorized green (red arrows, a normal ISLVs adjacent to an aISVs; blue arrows, a mislocalized ISLVs adjacent to a vISVs).

(L) Quantification of venous ISVs with an immediately adjacent ISLVs in uninjected embryos or embryos injected with constructs shown in (I) with or without TBF treatment. Values are the mean ± SEM.

(M) Quantification of arterial ISVs with an immediately adjacent ISLVs in uninjected embryos or embryos injected with constructs shown in (I), with or without TBF treatment. Values are the mean ± SEM. The total number of vISVs (L) or aISVs (M) counted is shown above each bar.

See also Figure S6.

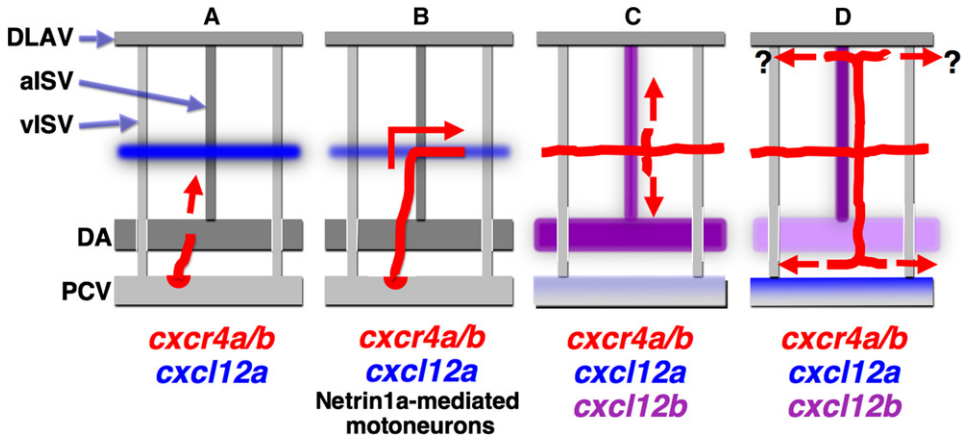

Figure 7. Proposed Model for Trunk Lymphatic Network Formation

Initial sprouting and dorsal migration of PCV-derived lymphatic progenitors (A) appear to occur independently of chemokine signaling, since sprouts form and migrate to the level of the HM without chemokine signaling. Cxcl12a guides Cxcr4a/b-expressing PCV-derived sprouting ECs into the superficial HM to form the PC (B). PC formation is also regulated by netrin1a-guided motoneuron axons in the HM, suggesting cooperative roles of chemokine and nonchemokine signaling mechanisms during PC formation. Cxcl12b-Cxcr4a/b signaling then guides dorsoventral growth of PC-derived lymphatic sprouts along aISVs but not vISVs (C). Finally, Cxcl12a and Cxcl12b direct TD formation in the space between the DA and PCV (D). The mechanism directing formation of the DLL adjacent to the DLAVs blood vessels is at present unknown. Red, developing lymphatics; red arrows, their growth direction.

As noted previously, PCV-derived lymphatic sprouts normally all turn laterally at the level of the HM, migrating toward the Cxcl12a-expressing superficial HM at the lateral surfaces, and do not grow further dorsally past the HM (Figures 1D–1K). As expected, lymphatic sprouts adjacent to FP cells expressing only TagRFP-T do not migrate dorsally past the HM (Figures 6B–6D and 6H). However, lymphatic sprouts near FP cells expressing both TagRFP-T and Cxcl12a frequently migrate dorsally past the HM toward the Cxcl12a-expressing cells (Figures 6E–6H), showing that Cxcl12a can direct migration of lymphatic progenitors.

As also noted above, ISLVs normally sprout from the PC adjacent to, and grow along, Cxcl12b-expressing aISVs but do not grow along Cxcl12b-negative vISVs (Figures 1S and 1T). Injection of a construct for mosaic, TBF-inducible expression of TagRFP-T alone in EC (Figure 6I) does not cause significant misalignment of ISLVs along vISVs following TBF treatment (Figure 6L). However, mosaic endothelial expression of TagRFP-T together with Cxcl12b results in frequent misalignment of ISLVs along vISVs (Figures 6J–6L; blue arrows in Figure 6K), without affecting the normal alignment of ISLVs along aISVs (red arrows in Figure 6K; Figure 6M). A low level of lymphatic misalignment along vISVs is seen in Cxcl12b expression construct-injected animals, even without TBF, but it is strongly increased by addition of TBF, confirming that misexpression of Cxcl12b is responsible for the misalignment phenotype (Figure 6L). Although embryos misexpressing cxcl12b throughout the vasculature show ectopic alignment of ISLVs along many vISVs (Figure 6L), the normal alignment of ISLVs along aISVs is not affected (Figure 6M), as might be expected, since the endogenous expression of cxcl12b in aISV has not been perturbed. This results in a somewhat increased total number of ISLVs in cxcl12b misexpressing animals. These results show that Cxcl12b can direct the alignment of lymphatics along BVs.

DISCUSSION

Properly directed and coordinated migration of ECs is essential for formation of stereotypic and evolutionarily conserved networks of blood and lymphatic vessels during development. Despite recent advances in our understanding of lymphatic development (Butler et al., 2009), the molecular mechanisms regulating lymphatic assembly and patterning remain largely undetermined. In this study, we provide evidence that chemokine signaling is critical for orchestrating the stepwise assembly of the trunk lymphatic vascular network (Figure 7). Cxcl12 (SDF1)-Cxcr4 chemokine signaling is required for multiple steps of trunk lymphatic network assembly. Cxcl12a-Cxcr4 signaling directs PCV-derived lymphatic progenitors (Figure 7A) to the superficial HM to form the PC, a transient endothelial cord containing the precursor cells for the developing trunk lymphatic network (Figure 7B). Cxcl12b-Cxcr4 signaling subsequently guides the dorsal and ventral growth of lymphatic precursors sprouting from the PC to form the ISLVs alongside aISVs (Figure 7C). Later, ventral expression of Cxcl12a in the PCV and Cxcl12b in the DA appears to mediate the alignment of the assembling TD between these two BVs (Figure 7D).

As described previously, primitive trunk vasculature in zebrafish is formed by DA-derived angiogenic "primary sprouts" and subsequent PCV-derived "secondary sprouts" (Isogai et al., 2003). Some of the secondary sprouts have an angiogenic fate, connecting with the primary sprouts to form vISVs. Other secondary sprouts adopt a lymphangiogenic fate, migrating further dorsally to the HM and contributing to the lymphatic PC. Our results show that Cxcr4 signaling is not required for the initial specification of Prox1-postive lymphatic progenitors or for their incorporation into secondary sprouts and dorsal migration to the level of the HM, because these early events occur normally in chemokine signaling-deficient animals (Figures 4D, 4F, 5H, and 7A; Figures S4B, S4H, and S5E). Although initial lymphatic

specification is intact, later lymphatic migration and patterning, such as PC formation along the superficial HM, are disrupted in chemokine-deficient animals (Figures 4D and 4F; Figures S4B and S4H). In addition, misexpression of Cxcl12a in the FP attracts ectopic migration of lymphangiogenic sprouts (Figures 6A–6H). Interestingly, previous studies have reported similar PC formation defects in zebrafish deficient in Netrin1a-Unc5b signaling (Navankasattusas et al., 2008; Wilson et al., 2006). Although a variety of studies have shown that Netrin acts as an antiangiogenic or repulsive factor for BV growth (Bouvrée et al., 2008; Larrivée et al., 2007; reviewed in Melani and Weinstein, 2010), other studies have reported an attractive guidance role, notably for zebrafish PC formation (Navankasattusas et al., 2008; Wilson et al., 2006). Like Cxcl12a, Netrin1a is also expressed along the superficial HM (Lauderdale et al., 1997), and deficiency of either Netrin1a, its presumptive receptor Unc5b, or Deleted in colorectal cancer (Dcc) results in loss of PC formation (Lim et al., 2011; Navankasattusas et al., 2008; Wilson et al., 2006). However, recent work has shown that Netrin1a signaling appears to be playing a nonautonomous role in PC formation and lymphatic patterning (Lim et al., 2011). The Dcc receptor is expressed in ventrally migrating motor neuron axons but not in migrating lymphatic endothelial progenitors, and Netrin1a and Dcc are required for motor axon positioning along the HM. Loss of these neurons through genetic or laser ablation results in defects in PC formation, suggesting that the motor neuron axons provide a cue (either direct or indirect) for PC alignment (Lim et al., 2011). Indeed, chemokine and netrin signaling appear to be required independently for PC formation (Figure 7B) because netrin1a MO injection does not alter the superficial HM expression of Cxcl12a, and vice-versa (unpublished data), but deficiency of these molecules together additively inhibits PC formation (Figure S5C).

LEC migration away from the PC is required for the formation of the trunk lymphatic vascular network, including the ISLVs, TD, and DLL (Figures 1L, 1P, 1S, 7C, and 7D). As we and others have reported previously (Bussmann et al., 2010; Geudens et al., 2010; Hogan et al., 2009; Küchler et al., 2006; Yaniv et al., 2006), LVs form along preexisting BVs, in particular arterial BVs. Sprouts emerge from the PC adjacent to, and then migrate dorsoventrally exclusively along, aISVs, avoiding vISVs (Figure 1T). The close anatomical association between ISLVs and aISVs suggests that arterial BVs provide a guidance cue for growing lymphatics. Indeed, we find that Cxcl12b ligand is expressed exclusively in aISVs at 3 dpf (Figures 3I–3M; Figures S3A and S3C–S3E), and Cxcl12b-deficient animals exhibit failure of both dorsal migration of LECs from the PC (Figures S4J–S4N) and formation of a ventral TD (Figure 4I) by 5 dpf, despite normal formation of the PC at earlier stages of development (Figure 4H). Furthermore, ectopic panendothelial expression of Cxcl12b promotes both ectopic migration of LECs and misalignment of ISLVs along vISVs (Figure 6I–6M; Figure S6), suggesting that Cxcl12b is the key molecule guiding LEC migration along aISVs (Figure 7C). A previous study examining the role of Notch signaling in zebrafish lymphatic development suggested that, in addition to its role in lymphatic emergence, Notch might also regulate lymphatic vessel pathfinding along arteries (Geudens et al., 2010). This result probably in large part reflects the requirement for Notch for artery specification. Notch-deficient animals form predominately vISVs instead of aISVs, depriving migrating LECs of most of their Cxcl12b-expressing arterial templates. However, these authors also observed a few cases in which lymphatic sprouts failed to migrate along or stalled during migration on "residual aISVs." Notch signaling appears to still be active in aISVs during LEC migration from the PC (Geudens et al., 2010), raising the possibility that Notch plays a more direct role in lymphatic pathfinding. In this regard, it would be important to determine whether Cxcl12b expression is reduced in the residual aISVs found in Notch-deficient animals, since our results suggest that Cxcl12b is both necessary and sufficient to direct ISLV-aISV alignment.

Later expression of Cxcl12a and Cxcl12b in the PCV and DA, respectively (Figure 3E–3J; Figure S3A–S3E), suggests that these ligands also guide the positioning of the TD. During TD assembly Cxcl12b expression in the DA is gradually decreasing, whereas Cxcl12a expression in the PCV is gradually increasing. This spatial-temporal gradient of chemokine ligand expression probably ensures that the final destination of ventrally migrating LECs is the area between DA and PCV (Figure 7D). The role of Cxcr4a/b-dependent signaling in DLL formation along the ventral surface of the DLAVs (Isogai et al., 2001) is less clear. Close apposition between the DLL and the DLAVs suggests that the DLAVs provide a guidance template for the DLL, but Cxcl12a and Cxcl12b expression is not detected in the DLAV at the level of detection of our WISH method.

Together, our results indicate that chemokine signaling plays a central role in directing trunk lymphatic vascular network assembly. Cxcr4-expressing LECs migrate to the superficial HM, along aISVs, and then between the DA and PCV by responding to Cxcl12 ligands (Figure 7). The blood endothelial expression of chemokine guidance cues is interesting in light of the well-documented common anatomical alignment of larger lymphatics with BVs, particularly arteries, throughout the vertebrates (Gray, 1918; Sabin, 1902, 1909). This suggests that the mechanisms described here may have wider implications for lymphatic patterning and LV growth, not only during embryogenesis but also during tumor-derived lymphangiogenesis. Recent studies have shown that the lymphatic vasculature is an important route for the metastatic spread of tumor cells (Achen et al., 2005; Alitalo et al., 2005; Wang and Oliver, 2010). Tumors actively induce both lymphangiogenesis and angiogenesis in the vicinity of tumors by secreting growth factors, such as VEGF-C, VEGF-D, and VEGF-A. Interestingly, many tumors are also known to express chemokine ligands and receptors in the tumor microenvironment, playing important roles in tumor-induced angiogenesis, tumor growth, and metastasis by autocrine and paracrine mechanisms (Raman et al., 2007; Somasundaram and Herlyn, 2009). For example, the CC chemokine receptor 7 (CCR7) in tumor cells responds to its ligand CCL21 in LEC, facilitating tumor cell invasion into LEC (Issa et al., 2009; Müller et al., 2001; Wiley et al., 2001). The identification of novel lymphatic guidance cues may therefore also lead to potential new clinical targets for lymphangiogenesis.

EXPERIMENTAL PROCEDURES

Zebrafish

Zebrafish (*Danio rerio*) embryos were obtained from natural spawning of laboratory lines. Embryos were raised and fish maintained as previously

described (Kimmel et al., 1995; Westerfield, 2000). Zebrafish lines used in the study are wild-type EK, *Tg(fli1a:EGFP)*^{y1} (Lawson and Weinstein, 2002), *cxcr4a*^{um21} (Bussmann et al., 2011), *medusa* (*cxcl12a*^{t30516}) (Valentin et al., 2007), and *cxcl12b*^{mu100} (Bussmann et al., 2011). Embryos were treated with 1-phenyl-2-thiourea (PTU) to inhibit pigment formation (Westerfield, 2000) to facilitate imaging and staining for whole-mount in situ hybridization (WISH). To immobilize embryos for imaging, they were treated with tricaine (Westerfield, 2000). Our zebrafish work was carried out under an approved animal protocol (Eunice Kennedy Shriver National Institute of Child Health and Human Development # 98-039).

Microscopy and Imaging

Embryos were mounted with 9% methyl cellulose for single time-point imaging. Embryos stained via WISH were imaged with a ProgRes C14 camera mounted on a Leica MZ12 stereomicroscope. High-magnification images were captured via a digital camera (The Imaging Source, Charlotte, NC, USA) mounted on an Olympus BX61WI compound microscope and iMovie program (Apple Inc., Cupertino, CA, USA). A movie showing blood flow was obtained from the digital camera (The Imaging Source) mounted on a Leica MZ FLIII stereomicroscope using iMovie (Apple Inc.). A Leica DC 500 digital camera mounted on a Zeiss Axioplan 2 compound microscope was used for obtaining images of sectioned *cxcl12a in situ*-stained embryos. Confocal microscopy images were acquired using a FluoView 1000 confocal microscope (Olympus, Center Valley, PA, USA) or a Leica SP5 inverted microscope (Leica Microsystems, Wetzlar, Germany). The images shown in this paper are single-view two-dimensional reconstructions of collected z-series stacks. Time-lapse imaging using two-photon microscopy (Zeiss LSM; Zeiss, Peabody, MA, USA) was performed as described previously (Kamei and Weinstein, 2005). Image z-stacks were collected using a *Tg(fli1a:EGFP)*^{y1} animal from 1.4 dpf (34 hpf) to 4.6 dpf (100 hpf), collecting images every 15–20 min. Each z-stack contains 54 sections collected 3 μm apart. Time-lapse movies were assembled using ImageJ (National Institutes of Health).

BAC Engineering using Homologous Recombination

To investigate the endogenous expression domains of chemokine ligand and receptor, we modified BAC clones containing genomic elements of Cxcl12b (ZC106B24) and Cxcr4a (ZH268G8) using homologous recombination (Figures S2A and S3B). Targeting vectors were made by Multisite Gateway Cloning (Invitrogen, Grand Island, NY, USA) and In-Fusion PCR Cloning System (Clontech, Mountain View, CA, USA). Each BAC clone was electroporated into *SW105* (Warming et al., 2005) and selected with chloramphenicol (12.5 ug/ml). The modified Cxcr4a BAC clone was further changed by inserting *iTol2* using homologous recombination (*iTol2*-Cxcr4a BAC; Suster et al., 2009). See Supplemental Experimental Procedures for targeting vector construction and homologous recombination.

Plasmid Constructs for In Situ RNA Probes

Because of high degree of identity in coding sequences between *cxcl12a* and *cxcl12b,* 3′ UTRs for each gene were amplified from stage-mixed cDNAs by PCR. A 324 bp PCR product for *cxcl12a* was generated with cxcl12aF (5′-AAAAAGCCCAACAGCAGCAGG-3′) and cxcl12aR (5′-ACACGGAGCAA ACAGGACTCC-3′) primers and cloned into pCRII-TOPO vector (Invitrogen). For *cxcl12b,* a 548-bp-long PCR product was amplified with cxcl12bF (5′-ATCCTTGCTTTGTGGTCCAG-3′) and cxcl12bR (5′-TAGCGTTGTGTGACC AGAGG-3′) and cloned into pGEM-T (Promega, Madison, WI, USA). For *cxcr4a,* cxcr4aF (5′-ACTTGCTGGAGACTGAAGGAG-3′) and cxcr4aR (5′-TGCAATGGTCTACATAAGTGC-3′) primer pairs were used to PCR amplify a portion of the coding sequence from stage mixed cDNAs. PCR products were inserted into the pCRII-TOPO vector.

Whole-Mount In Situ Hybridization and Section

RNA probes for *cxcl12a, cxcl12b, cxcr4a, cxcr4b,* and *prox1* were labeled with DIG and a probe for *dab2* with fluorescein using a DIG/fluorescein-labeling kit (Roche, Madison, WI, USA). WISH was carried out as described previously with some modifications (Hauptmann and Gerster, 1994). In some cases, to improve penetration of probes and color substrate in later-stage animals, fixed embryos were cut transversely across the head or trunk with a scalpel in 0.3 M sucrose solution before WISH procedure. For color staining, BM purple was used for DIG-labeled probes and INT/BCIP for the fluorescein-labeled probe. To better characterize the expression domain of *cxcl12a,* embryos stained with this probe were embedded with JB-4 plastic resin (Polysciences Inc., Warrington, PA, USA) and transverse sections (7–10 μM) were carried out using a microtome (Leica RM 2165, Leica, Wetzlar, Germany).

Microinjections

For the Cxcr4a rescue experiment, capped Tol2 transposase RNA (35 pg) and Tol2 plasmids (40 pg) containing a *fli1a*-derived promoter, EcRF′, and TagRFP-T or Cxcr4a-encoding sequences (see Figure 4L) were coinjected with 9 ng Cxcr4a MO into one blastomere of one-cell stage *Tg(fli1a:EGFP)*^{y1} embryos. For *cxcl12a* or *cxcl12b* ectopic expression experiments, capped Tol2 transposase RNA (35–50 pg) and Tol2 plasmids (35–50 pg) containing a tissue-specific promoter, EcRF′, and chemokine ligand-encoding sequences (see Figures 6A and 6I) were coinjected into the blastomere of one-cell stage *Tg(fli1a:EGFP)*^{y1} embryos. For visualization of Cxcr4a- or Cxcl12b-expressing cells, 100–150 pg of recombineered BAC DNA (see Figures S2A and S3B) was injected into the blastomeres of one-cell stage embryos. For the *iTol2*-Cxcr4a BAC, 70–80 pg BAC DNA was coinjected with capped Tol2 transposase RNA (40–50 pg) into the blastomeres of one-cell-stage embryos. Morpholinos (MOs; Gene Tools, Philomath, OR, USA) were injected into yolk of 1- to 2-cell-stage embryos. See Supplemental Experimental Procedures for MO sequences and the injection doses.

Inducible Overexpression Constructs

The Gal4-VP16-Ecdysone (GV-EcRF′):UAS system was utilized for spatiotemporal overexpression of chemokine ligands (Esengil et al., 2007). For expression of cxcl12a in neural floor plate (FP), shh promoter and FP-specific enhancer (Ar-B) in intron 1 was used (Ertzer et al., 2007). Ar-B (1329 bp) and shh promoter (2941 bp) fragments were separately amplified from an shh genomic DNA-containing BAC clone (ZC150E22) and connected to each other by overlapping PCR. The PCR product was cloned into pDONR P2R-P3 vector in an opposite direction. For expression of cxcl12b and Cxcr4a in EC, fli1ep fragment (Covassin et al., 2009) was cloned into pDONR P2R-P3 vector in an opposite direction. DNA fragments encoding either TagRFP-T only, or TagRFP-T and chemokine ligand-coding sequences (containing whole cDNA sequences, including N-terminal signal peptide-coding sequences), or TagRFP-T and Cxcr4a-coding sequences linked by a viral 2A peptide sequence (Provost et al., 2007; Szymczak et al., 2004) were amplified by overlapping PCR and cloned into pDONR 221. The complete inducible constructs were generated using Multisite Gateway Cloning (Invitrogen) and In-Fusion PCR Cloning System (Clontech). See Supplemental Experimental Procedures for inducible constructs.

Treatment of Cxcr4 Inhibitor and Tebufenozide

Cxcr4 antagonist TF10416 (4F-benzoyl-TN14003) (Tamamura et al., 2003a), a T140 analog, was provided by Dr. Nobutaka Fujii (Kyoto University, Kyoto, Japan). A stock solution for TF10416 was made by dissolving it in water at 10 mM concentration. To test Cxcr4 function in PC formation, embryos were incubated from 30 to 55 hpf in E3 embryo buffer (5 mM NaCl, 0.17 mM KCl, 0.33 mM $CaCl_2$, and 0.33 mM $MgSO_4$) containing 25–35 uM Cxcr4 inhibitor. The role of Cxcr4 in TD formation was tested by treating embryos from 3 to 5 dpf with 0.5–1 uM Cxcr4 inhibitor. Tebufenozide pestanal was purchased from Fluka, and a stock solution was made by dissolving it in dimethyl sulfoxide (DMSO; Sigma-Aldrich, St. Louis, MO, USA) at 50 mM concentration. Ecdysone was activated by incubating embryos with E3 embryo buffer containing 10–20 uM Tebufenozide (TBF). Buffer containing either Cxcr4 inhibitor or TBF was replaced daily. See Supplemental Experimental Procedures for more detail on TBF treatment.

Statistical Analysis

Data were evaluated with two-tailed unpaired Student's t test. Each value on graphs represents the mean ± standard error of the mean (SEM).

SUPPLEMENTAL INFORMATION

Supplemental Information includes six figures, Supplemental Experimental Procedures, and two movies and can be found with this article online at doi:10.1016/j.devcel.2012.01.011.

ACKNOWLEDGMENTS

We thank members of the Weinstein laboratory for technical help and critical suggestions. We would like to thank Dr. Nobutaka Fujii for providing the Cxcr4 inhibitor (TF10416). We are also grateful to James Chen for the gift of GV-EcRF′ plasmid. This research was supported by intramural program of the Eunice Kennedy Shriver National Institute of Child Health and Human Development and National Institutes of Health and by the Leducq Foundation. A.F.S. was supported by the Max Planck Society, a grant from the Deutsche Forschungsgemeinschaft (SI 1374/3-1), and an ERC starting grant (260794-ZebrafishAngio).

Received: May 27, 2011
Revised: November 7, 2011
Accepted: January 17, 2012
Published online: April 16, 2012

REFERENCES

Achen, M.G., McColl, B.K., and Stacker, S.A. (2005). Focus on lymphangiogenesis in tumor metastasis. Cancer Cell *7*, 121–127.

Alitalo, K., Tammela, T., and Petrova, T.V. (2005). Lymphangiogenesis in development and human disease. Nature *438*, 946–953.

Bouvrée, K., Larrivée, B., Lv, X., Yuan, L., DeLafarge, B., Freitas, C., Mathivet, T., Bréant, C., Tessier-Lavigne, M., Bikfalvi, A., et al. (2008). Netrin-1 inhibits sprouting angiogenesis in developing avian embryos. Dev. Biol. *318*, 172–183.

Bussmann, J., Bos, F.L., Urasaki, A., Kawakami, K., Duckers, H.J., and Schulte-Merker, S. (2010). Arteries provide essential guidance cues for lymphatic endothelial cells in the zebrafish trunk. Development *137*, 2653–2657.

Bussmann, J., Wolfe, S.A., and Siekmann, A.F. (2011). Arterial-venous network formation during brain vascularization involves hemodynamic regulation of chemokine signaling. Development *138*, 1717–1726.

Butler, M.G., Isogai, S., and Weinstein, B.M. (2009). Lymphatic development. Birth Defects Res. C Embryo Today *87*, 222–231.

Chong, S.W., Nguyet, L.M., Jiang, Y.J., and Korzh, V. (2007). The chemokine Sdf-1 and its receptor Cxcr4 are required for formation of muscle in zebrafish. BMC Dev. Biol. *7*, 54.

Christie, T.L., Carter, A., Rollins, E.L., and Childs, S.J. (2010). Syk and Zap-70 function redundantly to promote angioblast migration. Dev. Biol. *340*, 22–29.

Covassin, L.D., Siekmann, A.F., Kacergis, M.C., Laver, E., Moore, J.C., Villefranc, J.A., Weinstein, B.M., and Lawson, N.D. (2009). A genetic screen for vascular mutants in zebrafish reveals dynamic roles for Vegf/Plcg1 signaling during artery development. Dev. Biol. *329*, 212–226.

David, N.B., Sapède, D., Saint-Etienne, L., Thisse, C., Thisse, B., Dambly-Chaudière, C., Rosa, F.M., and Ghysen, A. (2002). Molecular basis of cell migration in the fish lateral line: role of the chemokine receptor CXCR4 and of its ligand, SDF1. Proc. Natl. Acad. Sci. USA *99*, 16297–16302.

Del Giacco, L., Pistocchi, A., and Ghilardi, A. (2010). prox1b Activity is essential in zebrafish lymphangiogenesis. PLoS ONE *5*, e13170.

Doitsidou, M., Reichman-Fried, M., Stebler, J., Köprunner, M., Dörries, J., Meyer, D., Esguerra, C.V., Leung, T., and Raz, E. (2002). Guidance of primordial germ cell migration by the chemokine SDF-1. Cell *111*, 647–659.

Ertzer, R., Müller, F., Hadzhiev, Y., Rathnam, S., Fischer, N., Rastegar, S., and Strähle, U. (2007). Cooperation of sonic hedgehog enhancers in midline expression. Dev. Biol. *301*, 578–589.

Esengil, H., Chang, V., Mich, J.K., and Chen, J.K. (2007). Small-molecule regulation of zebrafish gene expression. Nat. Chem. Biol. *3*, 154–155.

Fujita, M., Cha, Y.R., Pham, V.N., Sakurai, A., Roman, B.L., Gutkind, J.S., and Weinstein, B.M. (2011). Assembly and patterning of the vascular network of the vertebrate hindbrain. Development *138*, 1705–1715.

Geudens, I., Herpers, R., Hermans, K., Segura, I., Ruiz de Almodovar, C., Bussmann, J., De Smet, F., Vandevelde, W., Hogan, B.M., Siekmann, A., et al. (2010). Role of delta-like-4/Notch in the formation and wiring of the lymphatic network in zebrafish. Arterioscler. Thromb. Vasc. Biol. *30*, 1695–1702.

Ghysen, A., and Dambly-Chaudière, C. (2007). The lateral line microcosmos. Genes Dev. *21*, 2118–2130.

Gray, H. (1918). Anatomy of the Human Body (Philadelphia: Lea & Febiger).

Haas, P., and Gilmour, D. (2006). Chemokine signaling mediates self-organizing tissue migration in the zebrafish lateral line. Dev. Cell *10*, 673–680.

Hauptmann, G., and Gerster, T. (1994). Two-color whole-mount in situ hybridization to vertebrate and Drosophila embryos. Trends Genet. *10*, 266.

Hogan, B.M., Bos, F.L., Bussmann, J., Witte, M., Chi, N.C., Duckers, H.J., and Schulte-Merker, S. (2009). Ccbe1 is required for embryonic lymphangiogenesis and venous sprouting. Nat. Genet. *41*, 396–398.

Hollway, G.E., Bryson-Richardson, R.J., Berger, S., Cole, N.J., Hall, T.E., and Currie, P.D. (2007). Whole-somite rotation generates muscle progenitor cell compartments in the developing zebrafish embryo. Dev. Cell *12*, 207–219.

Isogai, S., Horiguchi, M., and Weinstein, B.M. (2001). The vascular anatomy of the developing zebrafish: an atlas of embryonic and early larval development. Dev. Biol. *230*, 278–301.

Isogai, S., Lawson, N.D., Torrealday, S., Horiguchi, M., and Weinstein, B.M. (2003). Angiogenic network formation in the developing vertebrate trunk. Development *130*, 5281–5290.

Issa, A., Le, T.X., Shoushtari, A.N., Shields, J.D., and Swartz, M.A. (2009). Vascular endothelial growth factor-C and C-C chemokine receptor 7 in tumor cell-lymphatic cross-talk promote invasive phenotype. Cancer Res. *69*, 349–357.

Kamei, M., and Weinstein, B.M. (2005). Long-term time-lapse fluorescence imaging of developing zebrafish. Zebrafish *2*, 113–123.

Kimmel, C.B., Ballard, W.W., Kimmel, S.R., Ullmann, B., and Schilling, T.F. (1995). Stages of embryonic development of the zebrafish. Dev. Dyn. *203*, 253–310.

Knaut, H., Werz, C., Geisler, R., and Nüsslein-Volhard, C.; Tübingen 2000 Screen Consortium. (2003). A zebrafish homologue of the chemokine receptor Cxcr4 is a germ-cell guidance receptor. Nature *421*, 279–282.

Küchler, A.M., Gjini, E., Peterson-Maduro, J., Cancilla, B., Wolburg, H., and Schulte-Merker, S. (2006). Development of the zebrafish lymphatic system requires VEGFC signaling. Curr. Biol. *16*, 1244–1248.

Larrivée, B., Freitas, C., Trombe, M., Lv, X., Delafarge, B., Yuan, L., Bouvrée, K., Bréant, C., Del Toro, R., Bréchot, N., et al. (2007). Activation of the UNC5B receptor by Netrin-1 inhibits sprouting angiogenesis. Genes Dev. *21*, 2433–2447.

Lauderdale, J.D., Davis, N.M., and Kuwada, J.Y. (1997). Axon tracts correlate with netrin-1a expression in the zebrafish embryo. Mol. Cell. Neurosci. *9*, 293–313.

Lawson, N.D., and Weinstein, B.M. (2002). In vivo imaging of embryonic vascular development using transgenic zebrafish. Dev. Biol. *248*, 307–318.

Lawson, N.D., Mugford, J.W., Diamond, B.A., and Weinstein, B.M. (2003). phospholipase C gamma-1 is required downstream of vascular endothelial growth factor during arterial development. Genes Dev. *17*, 1346–1351.

Lim, A.H., Suli, A., Yaniv, K., Weinstein, B., Li, D.Y., and Chien, C.B. (2011). Motoneurons are essential for vascular pathfinding. Development *138*, 3847–3857.

McKinney, M.C., and Weinstein, B.M. (2008). Chapter 4. Using the zebrafish to study vessel formation. Methods Enzymol. *444*, 65–97.

Melani, M., and Weinstein, B.M. (2010). Common factors regulating patterning of the nervous and vascular systems. Annu. Rev. Cell Dev. Biol. *26*, 639–665.

Müller, A., Homey, B., Soto, H., Ge, N., Catron, D., Buchanan, M.E., McClanahan, T., Murphy, E., Yuan, W., Wagner, S.N., et al. (2001). Involvement of chemokine receptors in breast cancer metastasis. Nature *410*, 50–56.

Nair, S., and Schilling, T.F. (2008). Chemokine signaling controls endodermal migration during zebrafish gastrulation. Science *322*, 89–92.

Navankasattusas, S., Whitehead, K.J., Suli, A., Sorensen, L.K., Lim, A.H., Zhao, J., Park, K.W., Wythe, J.D., Thomas, K.R., Chien, C.B., and Li, D.Y.

(2008). The netrin receptor UNC5B promotes angiogenesis in specific vascular beds. Development *135*, 659–667.

Ny, A., Koch, M., Schneider, M., Neven, E., Tong, R.T., Maity, S., Fischer, C., Plaisance, S., Lambrechts, D., Héligon, C., et al. (2005). A genetic Xenopus laevis tadpole model to study lymphangiogenesis. Nat. Med. *11*, 998–1004.

Oliver, G., and Alitalo, K. (2005). The lymphatic vasculature: recent progress and paradigms. Annu. Rev. Cell Dev. Biol. *21*, 457–483.

Pedrioli, D.M., Karpanen, T., Dabouras, V., Jurisic, G., van de Hoek, G., Shin, J.W., Marino, D., Kälin, R.E., Leidel, S., Cinelli, P., et al. (2010). miR-31 functions as a negative regulator of lymphatic vascular lineage-specific differentiation in vitro and vascular development in vivo. Mol. Cell. Biol. *30*, 3620–3634.

Provost, E., Rhee, J., and Leach, S.D. (2007). Viral 2A peptides allow expression of multiple proteins from a single ORF in transgenic zebrafish embryos. Genesis *45*, 625–629.

Raman, D., Baugher, P.J., Thu, Y.M., and Richmond, A. (2007). Role of chemokines in tumor growth. Cancer Lett. *256*, 137–165.

Sabin, F.R. (1902). On the origin of the lymphatic system from the veins and the development of the lymph hearts and thoracic duct in the pig. Am. J. Anat. *1*, 367–389.

Sabin, F.R. (1909). The lymphatic system in human embryos, with a consideration of the morphology of the system as a whole. Am. J. Anat. *9*, 43–91.

Saharinen, P., Helotera, H., Miettinen, J., Norrmen, C., D'Amico, G., Jeltsch, M., Langenberg, T., Vandevelde, W., Ny, A., Dewerchin, M., et al. (2010). Claudin-like protein 24 interacts with the VEGFR-2 and VEGFR-3 pathways and regulates lymphatic vessel development. Genes Dev. *24*, 875–880.

Siekmann, A.F., Standley, C., Fogarty, K.E., Wolfe, S.A., and Lawson, N.D. (2009). Chemokine signaling guides regional patterning of the first embryonic artery. Genes Dev. *23*, 2272–2277.

Somasundaram, R., and Herlyn, D. (2009). Chemokines and the microenvironment in neuroectodermal tumor-host interaction. Semin. Cancer Biol. *19*, 92–96.

Suster, M.L., Sumiyama, K., and Kawakami, K. (2009). Transposon-mediated BAC transgenesis in zebrafish and mice. BMC Genomics *10*, 477.

Szymczak, A.L., Workman, C.J., Wang, Y., Vignali, K.M., Dilioglou, S., Vanin, E.F., and Vignali, D.A. (2004). Correction of multi-gene deficiency in vivo using a single 'self-cleaving' 2A peptide-based retroviral vector. Nat. Biotechnol. *22*, 589–594.

Tamamura, H., Hiramatsu, K., Mizumoto, M., Ueda, S., Kusano, S., Terakubo, S., Akamatsu, M., Yamamoto, N., Trent, J.O., Wang, Z., et al. (2003a). Enhancement of the T140-based pharmacophores leads to the development of more potent and bio-stable CXCR4 antagonists. Org. Biomol. Chem. *1*, 3663–3669.

Tamamura, H., Hori, A., Kanzaki, N., Hiramatsu, K., Mizumoto, M., Nakashima, H., Yamamoto, N., Otaka, A., and Fujii, N. (2003b). T140 analogs as CXCR4 antagonists identified as anti-metastatic agents in the treatment of breast cancer. FEBS Lett. *550*, 79–83.

Tammela, T., and Alitalo, K. (2010). Lymphangiogenesis: Molecular mechanisms and future promise. Cell *140*, 460–476.

Tilney, N.L. (1971). Patterns of lymphatic drainage in the adult laboratory rat. J. Anat. *109*, 369–383.

Torres-Vázquez, J., Gitler, A.D., Fraser, S.D., Berk, J.D., Pham, V.N., Fishman, M.C., Childs, S., Epstein, J.A., and Weinstein, B.M. (2004). Semaphorin-plexin signaling guides patterning of the developing vasculature. Dev. Cell *7*, 117–123.

Valentin, G., Haas, P., and Gilmour, D. (2007). The chemokine SDF1a coordinates tissue migration through the spatially restricted activation of Cxcr7 and Cxcr4b. Curr. Biol. *17*, 1026–1031.

Wang, Y., and Oliver, G. (2010). Current views on the function of the lymphatic vasculature in health and disease. Genes Dev. *24*, 2115–2126.

Warming, S., Costantino, N., Court, D.L., Jenkins, N.A., and Copeland, N.G. (2005). Simple and highly efficient BAC recombineering using galK selection. Nucleic Acids Res. *33*, e36.

Westerfield, M. (2000). The Zebrafish Book: A Guide for the Laboratory Use of Zebrafish (*Danio rerio*), Fourth Edition (Eugene, OR: University of Oregon Press).

Wigle, J.T., and Oliver, G. (1999). Prox1 function is required for the development of the murine lymphatic system. Cell *98*, 769–778.

Wiley, H.E., Gonzalez, E.B., Maki, W., Wu, M.T., and Hwang, S.T. (2001). Expression of CC chemokine receptor-7 and regional lymph node metastasis of B16 murine melanoma. J. Natl. Cancer Inst. *93*, 1638–1643.

Wilson, B.D., Ii, M., Park, K.W., Suli, A., Sorensen, L.K., Larrieu-Lahargue, F., Urness, L.D., Suh, W., Asai, J., Kock, G.A., et al. (2006). Netrins promote developmental and therapeutic angiogenesis. Science *313*, 640–644.

Yaniv, K., Isogai, S., Castranova, D., Dye, L., Hitomi, J., and Weinstein, B.M. (2006). Live imaging of lymphatic development in the zebrafish. Nat. Med. *12*, 711–716.